At-wavelength figure metrology of hard x-ray focusing mirrors

Hirokatsu Yumoto,[a] Hidekazu Mimura, Satoshi Matsuyama, Soichiro Handa, and Yasuhisa Sano
Department of Precision Science and Technology, Graduate School of Engineering, Osaka University, 2-1 Yamada-oka, Suita, Osaka 565-0871, Japan

Makina Yabashi
SPring-8/Japan Synchrotron Radiation Research Institute (JASRI), 1-1-1, Kouto, Sayo-cho, Sayo-gun, Hyogo 679-5198 Japan

Yoshinori Nishino, Kenji Tamasaku, and Tetsuya Ishikawa
SPring-8/RIKEN, 1-1-1, Kouto, Sayo-cho, Sayo-gun, Hyogo 679-5198 Japan

Kazuto Yamauchi
Department of Precision Science and Technology, Graduate School of Engineering, Osaka University, 2-1 Yamada-oka, Suita, Osaka 565-0871, Japan

(Received 2 February 2006; accepted 31 May 2006; published online 30 June 2006)

We have developed an at-wavelength wave-front metrology of a grazing-incidence focusing optical systems in the hard x-ray region. The metrology is based on numerical retrieval from the intensity profile around the focal point. We demonstrated the at-wavelength metrology and estimated the surface figure error on a test mirror. An experiment for measuring the focusing intensity profile was performed at the 1-km-long beamline (BL29XUL) of SPring-8. The obtained results were compared with the profile measured using an optical interferometer and were confirmed to be in good agreement with it. This technique is a potential method of characterizing wave-front aberrations on elliptical mirrors for sub-10-nm focusing. © *2006 American Institute of Physics.*
[DOI: 10.1063/1.2216870]

I. INTRODUCTION

The availability of high-brilliance and coherent third-generation synchrotron radiation has allowed marked progress in analytical techniques in medicine, chemistry, materials science, and various other science fields. Scanning hard x-ray microscopy, microdiffraction, and spectromicroscopy using a hard x-ray microprobe have the ability to analyze materials nondestructively with precise spatial information. In these techniques, not only the focusing size of the hard x rays, but also the focusing intensity distribution properties determine the spatial and contrast resolution performances of the microscope used. An ideally focused beam, which is the so-called diffraction-limited focused beam, provides such microscopes with excellent resolution performances. A variety of optical devices have been developed to focus hard x rays using refraction, reflection, or diffraction effects. The focusing probes generated using Kirkpatrick-Baez (K-B) mirrors, which utilize two concave mirrors at a glancing angle to collect and focus x rays in both vertical and horizontal axes, have a high efficiency in comparison with other optics. A doubly focused full width at half maximum (FWHM) 36×48 nm^2 nearly diffraction-limited beam at 15 keV was obtained using K-B mirrors in the previous research of Mimura *et al.*[1]

The quality of the focusing probes is influenced by optical design, surface figure accuracy, the degree of coherence of illumination light, and alignment accuracy. We have developed the manufacturing process of directly figured elliptical mirrors for diffraction-limited focusing in hard x rays and applied them to a scanning x-ray microscope.[2–4] Computer-controlled plasma chemical vaporization machining[5] (PCVM) and elastic emission machining[6] (EEM) enable the figuring of mirror surfaces to a peak-to-valley (PV) accuracy better than 1 nm and a lateral resolution close to 0.1 mm.[1,7,8] In addition, surface figure metrology combining microstitching interferometry[9] (MSI) with relative angle determinable stitching interferometry[10] (RADSI) enable the measurement of the surface profile of an x-ray mirror to a PV accuracy better than 3 nm and a spatial resolution close to 10 μm.

To realize a smaller focusing size, mirrors with a larger numerical aperture (NA) are necessary. In this study, we designed a multilayer mirror for focusing hard x rays to a sub-10-nm size. As we will describe, we examined the acceptable tolerance of wave-front error to realize diffraction-limited sub-10-nm focusing. The wave-front aberration tolerance places extremely high demands on the fabrication of mirror substrates and multilayer coatings, and even higher demands on the metrology tools required to evaluate mirror surface qualities. Conventional surface metrologies are not sufficient. In the extreme ultraviolet (EUV) wavelength region, wave-front metrology is an essential tool for the development of diffraction-limited optical systems for lithography.[11] The system performance, composed of the geometric figure

[a]Author to whom correspondence should be addressed; electronic mail: yumoto@up.prec.eng.osaka-u.ac.jp

TABLE I. Optical parameters of designed mirror.

Mirror length	100 mm
Length of ellipse	500.075 m
Breadth of ellipse	135.9 mm
Focal length	150 mm
Glancing angle on optical axis	11.1 mrad
Acceptance width	1.1 mm
Surface coating	Graded Pt/C multilayer
Number of multilayer periods	20
Reflectivity in the first order on optical axis	60%
Double layer spacing (d spacing) on optical axis	3.7 nm

of the substrate surface and the properties of the multilayer coatings, is measurable only at the operational wavelength.

In this article, we suggest a new method of at-wavelength metrology for evaluating diffraction-limited focusing mirrors in the hard x-ray region. At-wavelength metrology for estimating the wave-front aberration of reflected x rays is based on numerical calculation using the intensity distribution around the focal point.

We demonstrated the at-wavelength metrology for a total-reflection mirror at 15 keV. The calculated profile was in good agreement with that measured by MSI, which indicates the effectiveness of the developed method.

II. DESIGN OF OPTICAL SYSTEM AND INVESTIGATION OF ACCEPTABLE TOLERANCE OF WAVE-FRONT ERROR FOR SUB-10-nm FOCUSING

We designed the line-focusing mirror with a large NA to have a 1.1 mm beam acceptance width and a 100-mm-long working distance, assuming application of this mirror in a microscope system. Table I lists the optical parameters of our focusing system. Figure 1 shows the figure profile of the designed mirror substrate. The substrate surface shape is part of an elliptical function in which one focal point is the light source and the other one is the focal point. The mirror was designed for the 1-km-long beamline[12] of SPring-8 where the mirror aperture can be coherently illuminated. The incidence angle on the optical axis is 11.1 mrad. By coating graded multilayers,[13,14] which fulfill the Bragg diffraction condition, a high reflectivity of 60% can be maintained at an incidence angle larger than the critical angle of the substrate material. Figure 2 shows the predicted intensity profile at a

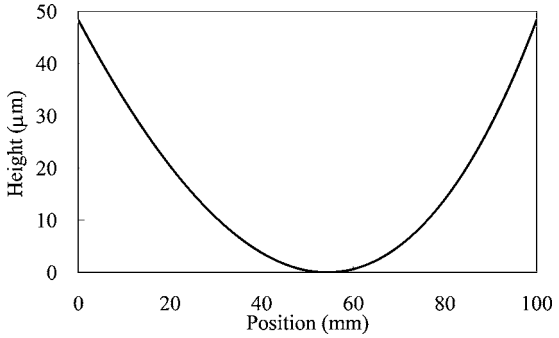

FIG. 1. Surface figure profile of designed mirror substrate for nanofocusing of hard x rays.

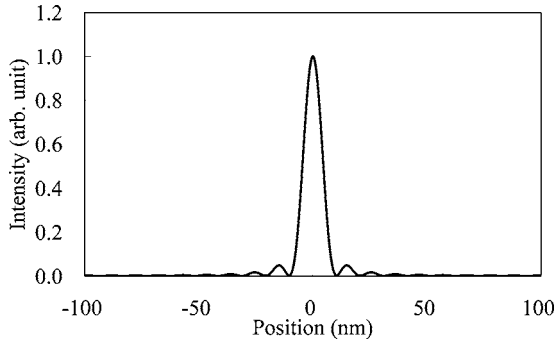

FIG. 2. Intensity profile of ideally focused x-ray beam at 15 keV, which is calculated using wave-optical simulator.

focal plane at 15 keV, which is obtained using a wave-optical simulator[2] coded on the basis of Fresnel-Kirchhoff diffraction integral theory. The ideal focusing size is 9.2 nm (FWHM).

We examined the acceptable tolerance of wave-front error to realize the diffraction-limited sub-10-nm focusing in this optical system. A wave-front accuracy of 1/4 λ (λ is the wavelength) is required in accordance with Rayleigh's quarter wavelength rule.[15] The wave-front error φ, attributed to the figure error height d, is expressed by the following equation in grazing-incidence total-reflection mirror optics:

$$\varphi = 2dk \sin \theta. \quad (1)$$

Here, θ is the glancing angle of an incident beam at the reflecting point, and k is the wave number. Wave-front error corresponds to the figure error in this optical system. The mutual relationships between the figure error characteristics and the focusing performances were investigated using the wave-optical simulator. Figure 3 shows the phase error profiles characterized in short, middle, and long spatial wavelength ranges in the longitudinal direction of the mirror. The PV phase error height is 1/4 λ, which is equal to a figure error height of 0.93 nm at the optical axis of this mirror. Figure 4 shows the calculated intensity profiles of focused x-ray beams using the elliptical mirror having the phase errors shown in Fig. 3. This simulation results indicate that the phase errors in the middle spatial wavelength range deform the shapes of the focal beam profiles and that the phase errors in the short spatial wavelength range decrease the inten-

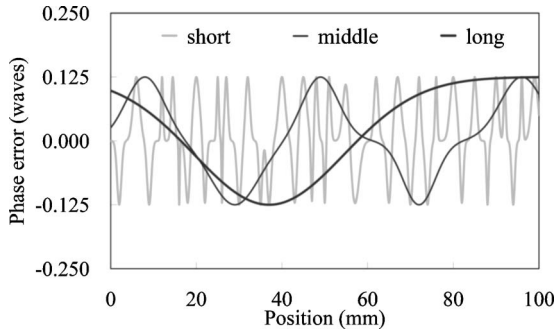

FIG. 3. Phase error profiles assumed on mirror surface characterized in short, middle, and long spatial wavelength ranges used in simulation for estimating wave-front aberration tolerance. PV phase error height corresponds to 1/4 λ.

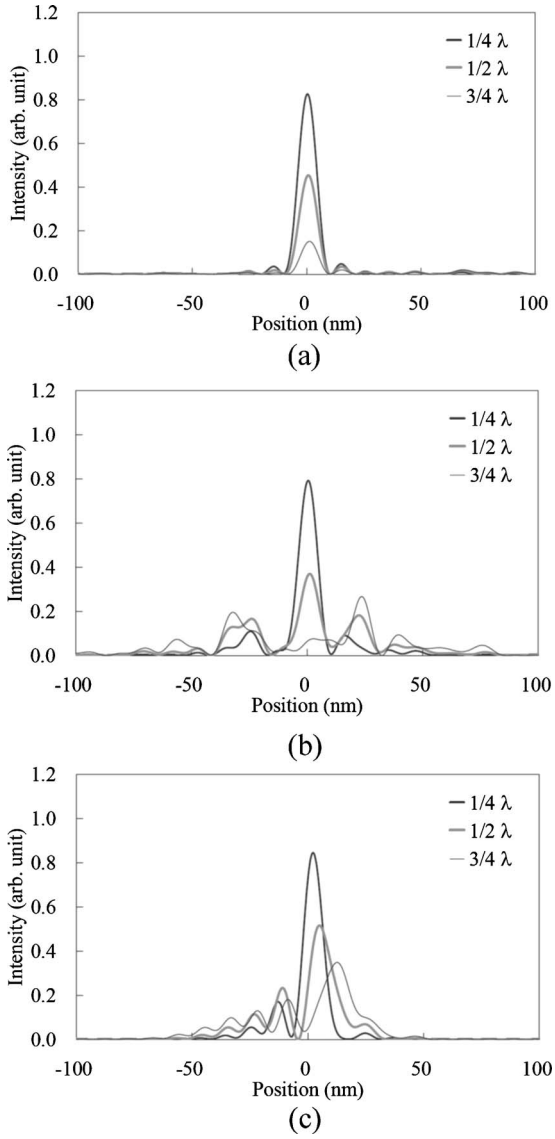

FIG. 4. Calculated intensity distribution profiles of focused x-ray beams using designed mirror having phase error height PV 1/4 λ, 1/2 λ, and 3/4 λ at an x-ray energy of 15 keV. (a) short, (b) middle, and (c) long spatial wavelength ranges.

sity of the focused beam. From these results, a PV figure error height of lower than 0.93 nm, corresponding to a phase error of 1/4 λ accuracy, is necessary for the metrology to realize the diffraction-limited focusing beam. Using the optical interferometer, the short spatial wavelength range is measurable with a 0.1 nm height accuracy. Metrology in the middle spatial wavelength range is desired.

III. AT-WAVELENGTH METROLOGY

We developed a method of evaluating the phase error of the focusing wave-front x ray due to the imperfections of the mirror. The observable physical value is the reflected intensity distribution from the test mirror without its phase information. Reconstructing the phase only from the intensity information is referred to as a phase problem. A Fourier-based iterative algorithm[16,17] and other algorithms[18,19] have been used to perform such a reconstruction. We developed two types of phase-retrieval algorithm in this study. One is based on an iterative-transform algorithm and the other is based on linear-optimization algorithms. In both retrieval programs, we applied the designed optical arrangement in our previously developed wave-optical simulator[2] to investigate the intensity distribution reflected by the mirror. Furthermore, we assumed a transverse coherence length of infinity at the light source in the model, because this enabled significant simplification of the algorithm. In the designed optical system, x rays illuminating the mirror are produced at an undulator and propagate for a long distance of 1 km. This designed optical system provides perfect coherent illumination on the mirror. The propagation of wave field $\Psi_0(r_0)$ on an s_0 screen at r_0 to $\Psi_1(r_1)$ on an s_1 screen is obtained as follows from the Fresnel-Kirchhoff diffraction formula:[20]

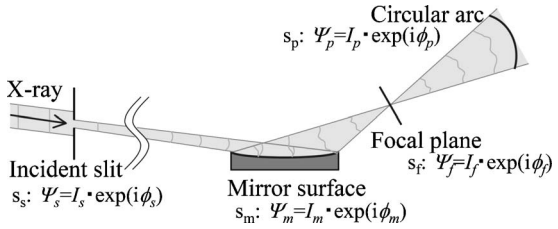

FIG. 5. Schematic of optical system for phase retrieval.

$$\Psi_1(r_1) = I_1(r_1)\exp(i\phi_1(r_1)) \tag{2}$$

$$= -\frac{i}{2\lambda}\int_{s_0} \Psi_0(r_0)\frac{\exp(ikr_{01})}{r_{01}}(1+\cos\chi)ds, \tag{3}$$

where $I_1(r_1)=|\Psi_1(r_1)|$ is the magnitude of the complex wave field, $\phi_1(r_1)$ is the phase of the wave field, $r_{01}=r_1-r_0$, and $-(i/2\lambda)(1+\cos\chi)$ is the inclination factor.[20] A wave field at focal plane Ψ_f is calculated using a wave field Ψ_m on the mirror surface. Ψ_m is calculated using a wave field Ψ_s on an incident slit.

A. Iterative-transform method

The wave-front error of the focusing beam is calculated on the basis of an error-reduction algorithm.[21] The mirror is assumed to shift the phase of the reflected wave and change the known intensity, because of its imperfections. The mirror acts as a pure phase object in the developed phase retrieval program. Wave-front error calculation is performed from a single intensity distribution. The intensities on the mirror and at the focal plane are sampled to satisfy the conditions of Nyquist's sampling theorem. We define a projection circular arc s_p. Figure 5 shows a schematic of the optical system for the phase retrieval. The phase retrieval problem is the recovery of phase ϕ_p on an s_p, which is equivalent to the wave-front phase error of the focusing beam, from the observed intensities I^2_{fexp} of the focal plane and I^2_{mexp} on the mirror surface. Figure 6 is a block diagram showing the phase retrieval algorithm. The phase retrieval algorithm consists of the following steps:

(0) Propagate through incident slit $s_s \rightarrow$ the mirror surface s_m: $\Psi_{m1}=I_{m1}\exp(i\phi_{m1})$. In this case, $\Psi_s=1$ is defined. The perfectly elliptical shape of the surface is taken as

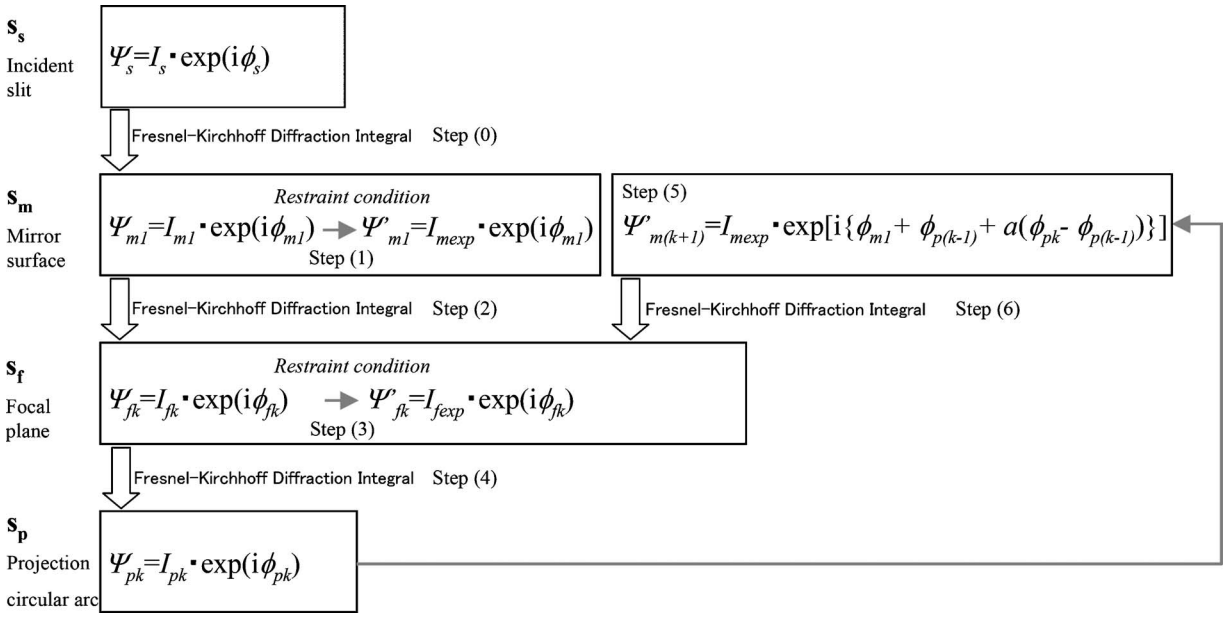

FIG. 6. Block diagram of phase retrieval algorithm.

the initial point of the iteration algorithm because the surface shape of the mirror can be measured approximately using the optical interferometer.

(1) The magnitude of Ψ_{m1} is replaced with the measured modulus I_{mexp}.
(2) Propagate s_m: $\Psi'_{m1} = I_{\mathrm{mexp}} \exp(i\phi_{m1}) \rightarrow$ the focal plane s_f: $\Psi_{fk} = I_{fk} \exp(i\phi_{fk})$. $k=1$.
(3) The magnitude of Ψ_{fk} is replaced with the measured modulus I_{fexp} at the kth iteration.
(4) Propagate s_f: $\Psi'_{fk} = I_{\mathrm{fexp}} \exp(i\phi_{fk}) \rightarrow s_p$: $\Psi_{pk} = I_{pk} \exp(i\phi_{pk})$.
(5) The phase of $\Psi_{m(k+1)}$ is replaced with $\{\phi_{m1} + \phi_{p(k-1)} + \alpha(\phi_{pk} - \phi_{p(k-1)})\}$. α, the step size, is a positive constant. $[\phi_{p(k-1)} = 0$ at $k=1.]$
(6) Propagate s_m: $\Psi'_{m(k+1)} = I_{\mathrm{mexp}} \exp[i\{\phi_{m1} + \phi_{p(k-1)} + \alpha(\phi_{pk} - \phi_{p(k-1)})\}] \rightarrow s_f$: $\Psi_{f(k+1)} = I_{f(k+1)} \exp(i\phi_{f(k+1)})$.

Then, steps (3)–(6) are repeated to obtain a consistent ϕ_p. In step (4), the wave-front error on the mirror surface is calculated. We assume the wave-front of the focusing wave to be of the same form and independent of the distance from the focal point if the distance is sufficiently large, because the wave-front error under consideration is sufficiently small.

Simulation was performed to explore the characteristics of the phase retrieval algorithm. The simulated optical system is designed to achieve sub-10-nm focusing, and the assumed phase error on the mirror surface is shown in Fig. 8(a). Figure 7 shows the focusing intensity profiles recovered [Fig. 7(b)] and set as the original value [Fig. 7(a)]. Figure 8(b) shows the recovered phase error on the ideal surface curve. Approximately 1000 iterations were performed to obtain the result. From the intensity profile, including no measurement noise, an accuracy on the order of 0.023 waves rms was simulated under these conditions.

The Fourier transform of the complex amplitude distribution of the focusing light wave becomes a complex amplitude distribution at the focal plane. From this viewpoint, the intensity distribution around the focal point is more sensitive to the middle and long spatial wavelength ranges than to the short range. This wave-front metrology has a higher potential for evaluating focusing optics than an optical interferometer.

B. Linear-optimization method

The other approach to determining wave-front error is the iteration method, which minimizes the differential inten-

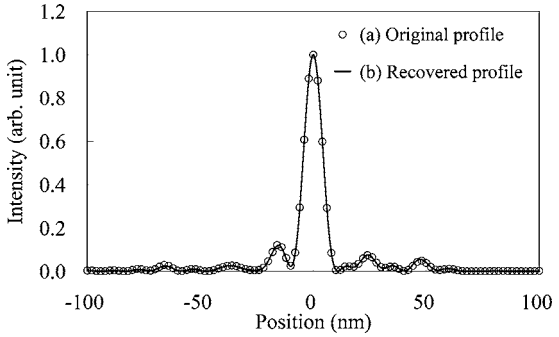

FIG. 7. Results of numerical simulation of phase retrieval algorithm. Intensity distribution profiles at focal point. (a) Original intensity profile. (b) Reconstructed intensity profile.

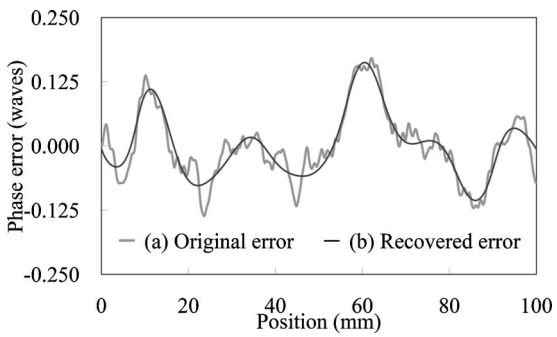

FIG. 8. Results of numerical simulation of phase retrieval algorithm. Phase error distribution on ideally shaped mirror surface. (a) Original phase error. (b) Phase error distribution reconstructed from intensity at focal point.

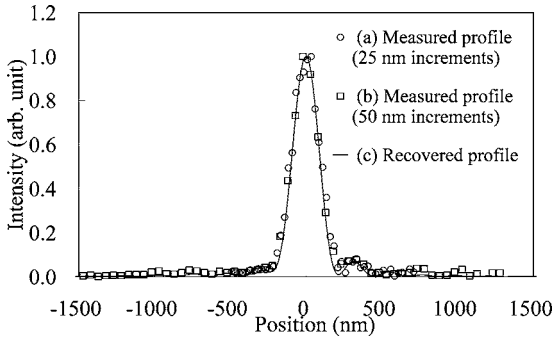

FIG. 9. Experimental results of at-wavelength metrology. Intensity distribution profiles at focal point at an x-ray energy of 15 keV. [(a) and (b)] Measured intensity profile using wire-scanning method. (a) Open circles denote 25 nm increments and (b) open squares denote 50 nm increments. (c) Reconstructed intensity profile using phase retrieval algorithm.

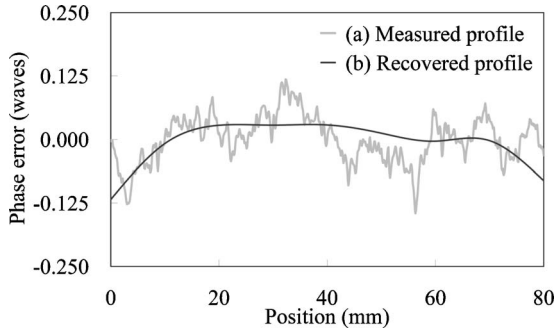

FIG. 10. Experimental results of at-wavelength metrology. Phase error distribution on ideal shape plane of focusing mirror. (a) Measured profile using optical interferometer. (b) Reconstructed profile from measured intensity profile at focal point.

sity between experimental and simulated data by solving a direct problem.[2] A wave-front error is expressed as a weighting function of unit phase error. The error parameters are composed of PV height and spatial wavelength in the longitudinal direction of the mirror. This method allows us to find the solution even if the measured intensities contain noise. One of the main problems of this phase retrieval method is the long computation time. To overcome this difficulty, the coded program is substantially simplified. The iterative procedure is continued until no further improvement is observed.

To avoid the local minimum problem, the two developed algorithms are combined to calculate wave-front error using the measured intensity distribution. Additional intensity measurements around the focal point are of assistance in performing high-precision computation.

IV. EXPERIMENT AND RESULTS

At-wavelength wave-front metrology for a total reflection mirror at 15 keV was demonstrated. The experiment was performed using the 1-km-long beamline (BL29XUL) of SPring-8. The test mirror has a much smaller NA than the designed sub-10-nm focusing mirror. The test mirror surface can be measured with a high accuracy by MSI and a focusing intensity profile of 200 nm (FWHM) can be detected accurately by a wire scanning method. The optical parameters and the shape of the test mirror are given elsewhere.[22] Figure 9 shows [Figs. 9(a) and 9(b)] the measured intensity profiles, and [Fig. 9(c)] the recovered intensity profile using the retrieval algorithm at the focusing point. The intensity profiles were measured at 25 and 50 nm intervals independently. Figure 10 shows the phase error profiles on the test mirror surface [Fig. 10(a)] measured by MSI and [Fig. 10(b)] recovered using the retrieval algorithm. In this optical system, the phase error of $1/4\ \lambda$ corresponds to a figure error height of 7.4 nm at the mirror center. Although the retrieval accuracy depends on the precision of the intensity measurement of the focusing beam, the difference in wave-front error between the two phase errors is 0.052 waves rms. The good agreement between the two figure error profiles in the middle spatial wavelength range proves the high capability of the developed metrology, not shared by conventional surface metrologies, to realize diffraction-limited focusing.

We have developed and demonstrated efficient at-wavelength wave-front metrology. Realization of the sub-10-nm diffraction-limited focusing requires a manufacturing process consisting of the at-wavelength assessment of the fabricated mirror and the phase correction of wave-front aberration on the basis of the estimated phase error. Therefore, the at-wavelength wave-front metrology presented here is an indispensable tool. The phase correction of the multilayer mirror in the hard x ray region is shown possible by an additional deposition method.[14] One of the technical considerations of the process is the accuracy of the characterizing method for the sub-10-nm focusing intensity distribution. Several techniques have been used to evaluate the nanobeams,[23–25] however, these have not been demonstrated in the sub-10-nm region.

At-wavelength wave-front metrology is also applicable to microdiffraction, in which the illuminated x-ray wave front over the object must be known. Sub-10-nm hard x-ray probes with extremely intense light will revolutionize the field of microscopy. This technique offers the ability to realize nondestructive analyses of the internal structure of materials with the same spatial resolution as electron microscopy and AFM (atomic force microscopy), and moreover, to realize monomolecular resolution analyses.

ACKNOWLEDGMENT

This research was supported by Grant-in-Aid for Scientific Research (S), 15106003, 2004 and the 21st Century COE Research, Center for Atomistic Fabrication Technology, 2004 from the Ministry of Education, Sports, Culture, Science and Technology.

[1] H. Mimura *et al.*, Jpn. J. Appl. Phys., Part 1 **44**, 539 (2005).
[2] S. Matsuyama *et al.*, Rev. Sci. Instrum. **76**, 083114 (2005).
[3] H. Yumoto *et al.*, Rev. Sci. Instrum. **76**, 063708 (2005).
[4] S. Matsuyama *et al.*, Proc. SPIE **5918**, 591804 (2005).
[5] K. Yamamura *et al.*, Rev. Sci. Instrum. **74**, 4549 (2003).
[6] K. Yamauchi, H. Mimura, K. Inagaki, and Y. Mori, Rev. Sci. Instrum. **73**, 4028 (2002).
[7] H. Mimura *et al.*, J. Synchrotron Radiat. **11**, 343 (2004).
[8] K. Yamauchi *et al.*, Jpn. J. Appl. Phys., Part 1 **42**, 7129 (2003).
[9] K. Yamauchi *et al.*, Rev. Sci. Instrum. **74**, 2894 (2003).
[10] H. Mimura *et al.*, Rev. Sci. Instrum. **76**, 045102 (2005).

[11] H. Medecki, E. Tejnil, K. A. Goldberg, and J. Bokor, Opt. Lett. **21**, 1526 (1996).
[12] K. Tamasaku, Y. Tanaka, M. Yabashi, H. Yamazaki, N. Kawamura, M. Suzuki, and T. Ishikawa, Nucl. Instrum. Methods Phys. Res. A **467–468**, 686 (2001).
[13] Ch. Morawe, P. Pecci, J. Ch. Peffen, and E. Ziegler, Rev. Sci. Instrum. **70**, 3227 (1999).
[14] S. Handa *et al.*, Nucl. Instrum. Methods Phys. Res. A (submitted).
[15] M. Born and E. Wolf, *Principles of Optics*, 7th ed. (Cambridge University Press, Cambridge, 2001), p. 528.
[16] J. Miao, P. Charalambous, J. Kirz, and D. Sayre, Nature (London) **400**, 342 (1999).
[17] Y. Nishino, J. Miao, and T. Ishikawa, Phys. Rev. B **68**, 220101 (2003).
[18] A. Souvorov, M. Yabashi, K. Tamasaku, T. Ishikawa, Y. Mori, K. Yamauchi, K. Yamamura, and A. Saito, J. Synchrotron Radiat. **9**, 223 (2002).
[19] J. R. Fienup, Appl. Opt. **32**, 1737 (1993).
[20] M. Born and E. Wolf, *Principles of Optics*, 7th ed. (Cambridge University Press, Cambridge, 2001), pp. 422–423.
[21] J. R. Fienup, Appl. Opt. **21**, 2758 (1982).
[22] K. Yamauchi *et al.*, J. Synchrotron Radiat. **9**, 313 (2002).
[23] Y. Suzuki, A. Takeuchi, H. Takano, and H. Takenaka, Jpn. J. Appl. Phys., Part 1 **44**, 1994 (2005).
[24] W. Liu, G. E. Ice, J. Z. Tischler, A. Khounsary, C. Liu, L. Assoufid, and A. T. Macrander, Rev. Sci. Instrum. **76**, 113701 (2005).
[25] O. Hignette, P. Cloetens, G. Rostaing, P. Bernard, and C. Morawe, Rev. Sci. Instrum. **76**, 063709 (2005).